

Flight Test and Validation of Variable Coded Modulation Using SCan Testbed

Hua Xie*, Sam Dolinar*, Matthew Chase[†], Susan Clancy[†], Michael Kilzer[‡], Leigh Torgerson*, and Andre Tkacenko*

ABSTRACT. — This article reports on the development and validation of variable coded modulation (VCM) on the Jet Propulsion Laboratory (JPL) software-defined radio (SDR). Flight tests were conducted to evaluate performance of the VCM waveform over an S-band link between the Space Communications and Navigation (SCaN) Testbed and the Glenn Research Center (GRC). The tests verified the VCM waveform’s ability to switch to different modulation and coding modes adapting to varying link conditions, and demonstrated improvement in effective data throughput as compared to NASA standard waveforms. We also describe a suite of ground receiver tools that were developed to autonomously acquire, track, and post-process the JPL VCM waveform. Processing results from one of the tests indicate an overall improvement of ~ 2 dB in data throughput over standard waveforms. The demonstrated technologies are building blocks of a future cognitive radio system with the capability to adapt its operation to the communication environment in near real time.

I. Introduction

Variable Coded Modulation (VCM) methods allow users to change coding and modulation during a communication session to adapt the transmitted information data rate to dynamic link conditions. Compared to traditional communication systems that use constant coding and modulation designed for worst-case link conditions, VCM can significantly increase overall effective data throughput when the radio is configured adaptively to fully utilize link capacity.

*Communications Architectures and Research Section.

[†]Flight Communications Systems Section.

[‡]Tracking Systems and Applications Section.

The research described in this publication was carried out by the Jet Propulsion Laboratory, California Institute of Technology, under a contract with the National Aeronautics and Space Administration. © 2017 California Institute of Technology. Government sponsorship acknowledged.

Several classes of channel codes and modulations have been recommended by the Consultative Committee for Space Data Systems (CCSDS) for use in space-to-Earth links. The first of these standards [1] includes convolutional codes, Reed-Solomon codes, turbo codes, and low-density parity-check (LDPC) codes to be used with binary phase shift keying (BPSK), quadrature phase shift keying (QPSK) or offset QPSK (OQPSK), and Gaussian minimum shift keying (GMSK) modulations as recommended in [2]; A second CCSDS Blue Book [3] recommends a set of serially concatenated convolutional codes (SCCCs) together with QPSK, 8-ary phase shift keying (8-PSK), and 16-ary, 32-ary, and 64-ary amplitude and phase shift keying (16-APSK, 32-APSK, 64-APSK, respectively) modulations. A VCM protocol is also recommended in the same Blue Book. A third Blue Book [4] specifies a mechanism to communicate CCSDS frames using the European Telecommunications Standard Institute (ETSI) Digital Video Broadcasting by satellites (DVB-S2) second-generation standard [5]. Since commercial receiver equipment exists for DVB-S2, it was adopted in a VCM experiment performed by Glenn Research Center (GRC) [6].

Currently each of these coded modulation schemes, i.e., [1], [3], [4], are stovepipes and do not relate or refer to each other. A general CCSDS VCM protocol [7] provides a unified approach to mix and match these codes and modulations for an application that is understandable to the receiver. In this article we report on the development, validation, and flight test of a JPL VCM waveform that combines telemetry turbo and LDPC codes [1] with modulations in [2] using the VCM protocol in [7]. The JPL VCM waveform consists of both software and firmware components. Our current version has the encoder and bit randomizer implemented in software. The VCM frame slicer, header insertion, and modulation are all implemented in a field programmable gate array (FPGA).

We developed a suite of ground receiver tools to acquire, track, and post-process the JPL VCM waveform. Link predictions were used to generate a VCM coding and modulation profile that aims at maximizing utilization of link capacity. This profile was translated into a time-triggered script and uploaded to the SCaN Testbed onboard the International Space Station (ISS) to configure the software-defined radio (SDR). The flight tests were performed using the S-band link between the SCaN Testbed and the ground station at GRC. Running the tests using ISS links provides a real-world interference scenario to evaluate the benefits of VCM methods. This technology demonstration could be a precursor to a closed-loop adaptive coded modulation (ACM) scheme that would be able to autonomously adapt the radio configuration using uplink feedback information on link conditions.

The article is organized as follows. Section II describes the development and validation of JPL's VCM waveform on a software-defined radio prototype located in Building 114 of JPL. Section III reports on the flight tests that were performed using the SCaN Testbed, including test goals, link predictions, ground integration preparation tests, and hardware/software configurations. Section IV presents the flight test results, including waveform validation and performance analysis.

II. JPL VCM Waveform Development on Software-Defined Radio

The JPL VCM waveform implements the set of CCSDS turbo and LDPC codes [1] and modulation options including BPSK, QPSK, 8-PSK, 16-amplitude phase shift keying (16-APSK), 32-APSK, and 64-APSK, as recommended in [2]. Transmitted data consist of a sequence of contiguous physical layer (PL) frames, sliced and formed according to the VCM protocol [7]. The generation and structure of the VCM frames are shown in Figure 1 (copied from [7]).

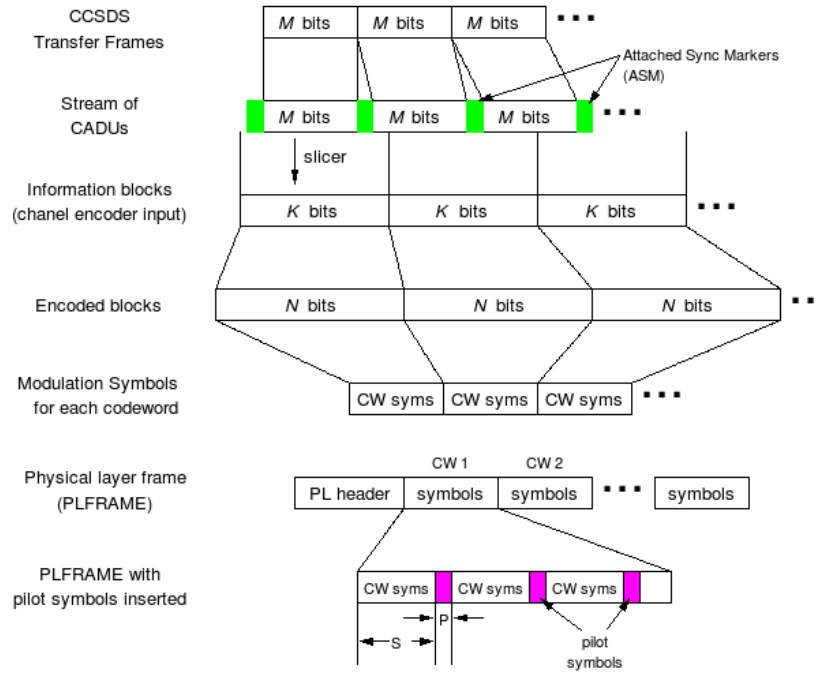


Figure 1. Structure of the physical layer frames of the VCM protocol [7].

We implemented the VCM protocol by taking the streams of input data (i.e., channel access data units (CADUs)), slicing them into blocks of K bits (encoder input size), encoding each input block, producing modulation symbols, and prepending the VCM frame header to the modulated symbols. The VCM frame header consists of the attached synchronization marker (ASM) and the frame descriptor, transmitted using $\pi/4$ BPSK, to enable VCM frame synchronization and mode detection. The receiver locates/decodes the frame descriptors and configures the demodulator and decoder accordingly to acquire and recover information data blocks.

In this article, we report the test results of VCM modes 0 to 15 for CCSDS turbo and LDPC codes [7]. Coding and modulation options for these modes are shown in Table 1. The (8160,7136) C2 code is an expurgated, shortened, and extended version of a basic (8176,7156) LDPC code, with C2 referring to the code construction method [8]. Long block length codes and higher order modulation techniques, i.e., 16-APSK, 32-APSK, and 64-APSK, are being developed and are planned to be evaluated in future flight

tests. Our current waveform version prepends a VCM physical layer (PL) header to each modulated codeword. In Table 1, we include both the input length (bits) and output modulated codeword length (symbols).

Table 1. VCM modes that have been implemented and tested using the SCaN Testbed.

VCM Mode	Modulation	Code	Code Rate	Input length (bits)	Output length (symbols)
0	BPSK	None		1024	1024
1	BPSK	Turbo	1/6	1784	10752*
2	BPSK	Turbo	1/4	1784	7168*
3	BPSK	Turbo	1/3	1784	5376*
4	BPSK	AR4JA LDPC	1/2	1024	2048
5	BPSK	AR4JA LDPC	2/3	1024	1536
6	BPSK	AR4JA LDPC	4/5	1024	1280
7	BPSK	C2	223/255	7136	8160
8	QPSK	AR4JA LDPC	1/2	1024	1024
9	QPSK	AR4JA LDPC	2/3	1024	768
10	QPSK	AR4JA LDPC	4/5	1024	640
11	QPSK	C2	223/255	7136	4080
12	8-PSK	AR4JA LDPC	1/2	1024	683**
13	8-PSK	AR4JA LDPC	2/3	1024	512
14	8-PSK	AR4JA LDPC	4/5	1024	427**
15	8-PSK	C2	223/255	7136	2720

* The current version of the VCM waveform software generates VCM frames with output lengths in multiples of 32 bits. This limitation will be resolved in the next waveform version.

** Zero padding is applied to the end of each VCM frame to produce an integer number of modulated symbols.

The JPL software-defined radio (SDR) generates waveforms making use of software and reconfigurable hardware devices implemented in a field programmable gate array (FPGA). Figure 2 shows the functional block diagram of VCM waveform generation. Our current version of the waveform has the slicer, encoder, and randomizer implemented in software. An interface between the software and the FPGA exists to transfer data to the first-in first-out (FIFO) buffer and to configure the FPGA. The FPGA design targets the QRVirtex-II present in the JPL SDR on the SCaN Testbed. This design can be ported to other Xilinx FPGA devices. In this test we used an 8-bit ramping test pattern as input information data stream, repeated and sliced according to the specified input block length of the VCM mode being tested. In order to maintain sufficient bit transition density in the received codewords for symbol timing acquisition, we applied bit randomization to each VCM codeword by exclusive-ORing (XOR) with the CCSDS standard pseudo-random sequence [9].

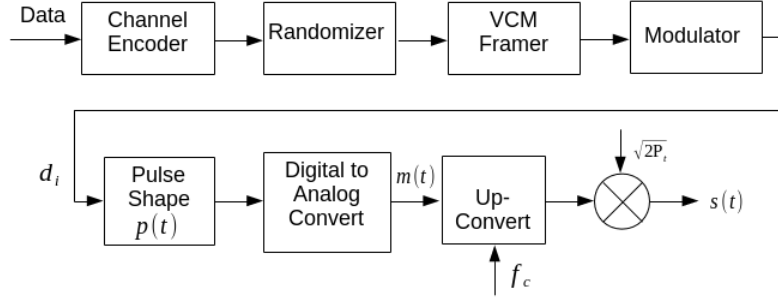


Figure 2. Block Diagram of VCM waveform generation (see Equation (1) for definition of $s(t)$, $m(t)$, and $p(t)$).

The FPGA reads the encoded and randomized data from the FIFO and performs VCM framing and modulation based on the user configured VCM mode. For example when software configures the FPGA to use VCM mode 4 with rate 1/2 LDPC code and BPSK modulation, codewords will be fetched from FIFO, sliced into 2048-bit blocks, modulated using $\pi/4$ BPSK modulation, and prepended with the VCM frame header. Generation of the VCM frame header is described in [7] and is compatible with the SCCC VCM protocol [3]. More specifically for the tests conducted, we adopted the SCCC 256-bit frame marker and used a Reed-Muller code to construct the 64-bit frame descriptors. The software ensures that the FIFO does not encounter overflow or underflow conditions and orchestrates the switching of VCM modes.

One limitation of our current waveform version is that software encoding is not able to keep up with the FPGA throughput. As a result, FIFO underflow will occur during mode transitions when the FIFO is waiting for software to queue up encoded data. As a temporary fix to this issue, the VCM software monitors the FIFO constantly and configures the FPGA to use its internally generated pseudorandom binary sequence (PRBS) data and transmit them using VCM mode 0 (dummy frames) when there is not enough data in the FIFO. This limitation leads to overhead in data transmission and reduces effective data throughput. Our next version of VCM waveform will have encoding and randomization implemented in the FPGA and therefore will no longer need to transmit VCM mode 0 frames during mode transitions.

A. The SDR's Modulator Calibration and Continuous Wave Inteferecence

The bit streams of the encoded blocks are mapped to in-phase and quadrature (I/Q) components in the vector modulator, i.e., the I/Q modulator of the SDR. The modulated pulses are then passed to the digital-to-analog converters (DACs) and mixed with the carrier with frequency centered at f_c . The complex representation of the transmitted downlink signal is of the form presented in Equation (1)

$$s(t) = \sqrt{2P_t}m(t)e^{j2\pi f_c t}, \quad (1)$$

where

P_t is the total signal power

f_c is the carrier frequency in Hz

$$m(t) = \sum_{i=-\infty}^{\infty} d_i p(t - iT)$$

d_i is the i th modulated symbol (complex)

T is the symbol duration

$p(t)$ is a pulse-shape defined over the interval $[0, T]$, and

t is time in seconds.

Ideally the outputs from the modulator are centered around a midpoint in the DAC's possible value range. However, there exists an imbalance between the I/Q modulators of the SDR. Proper adjustments must be performed before mixing the modulator outputs with the carrier for transmission. Without proper calibration, a DC offset will occur in the signal and manifest itself as continuous wave interference in the received signal when the SDR transmit frequency deviates from the center frequency of the downlink S-band.

We assume that the JPL SDR's radio frequency (RF) is centered at f_s and is shifted Δf away from the tuned S-band downlink frequency, f_c , of the receiver at GRC. In operation, the modulator outputs are first mixed with this frequency offset Δf and then adjusted for DC offset. When the vector modulator is not fully calibrated, the mixed signal will contain both the modulated signal component at the frequency offset Δf and a DC component

$$m'(t) = \sqrt{2I_d}e^{j\theta_d} + \sqrt{2P_t}e^{j(2\pi\Delta ft + \phi(t))}, \quad (2)$$

where $\sqrt{2I_d}e^{j\theta_d}$ is the complex representation of the DC component and $\phi(t)$ is the phase of the modulated signal.

After mixing $m'(t)$ with the SDR RF at f_s , we obtain the transmitted signal in the following form as given by Equation (3)

$$s'(t) = \sqrt{2I_d}e^{j(2\pi f_s t + \theta_d)} + \sqrt{2P_t}e^{j(2\pi f_c t + \phi(t))}, \quad (3)$$

At the receiver, we use a local oscillator with center frequency f_c to down-convert the received signal. The output signal from the down-conveter is represented as

$$r(t) = \sqrt{2I_d}e^{j(2\pi\Delta ft + \theta_d)} + \sqrt{2P_t}e^{j\phi(t)} + n_i(t), \quad (4)$$

where Δf is the frequency offset and $n_i(t)$ is the additive noise from the channel and from the receiver. The first term in Equation (4) represents a continuous wave (CW) interference. In our case, this CW interference was caused by a combination of carrier frequency offset and uncalibrated DC offset/imbalance in the SDR modulator. The CW interference will lead to degradation of carrier tracking loop performance [10, 11]. The

tracking performance is dependent on the signal-to-interference power ratio P_t/I_d , the noise level, and the carrier frequency offset Δf . An approximate analytical model was developed in [10] for the phase error process when the frequency offset of the interferer exceeds the loop filter bandwidth. Conditions under which the tracking loop can acquire the desired signal were derived. When the noise level exceeds a certain threshold above the signal and interferer, the average phase error rate, which represents the average number of cycles the numerically controlled oscillator (NCO) has changed from its initial state per unit time, equals the residual frequency. In this case the desired signal cannot be tracked. Conversely, the average phase error rate approaches zero for low noise level, and the tracking loop reaches a steady state and remains in lock.

In fact, the calibration parameters (I/Q gain and phase offset) are specific to each instance of the SDR radio. In particular, the vector modulator in the laboratory breadboard (also referred to as the JPL SDR prototype) is very different from the one used in the engineering model (EM) at GRC and the flight model (FM) onboard the ISS. During development of the JPL VCM waveform, we adjusted these parameters based on the prototype SDR. On the first day of our flight test, these values were not calibrated to match the values of the SDR flight model. This miscalibration resulted in CW interference in received signal and caused data loss in the first few passes. In Section IV-C, we report on the data losses of a pass where the CW interference was present due to miscalibration of the vector modulator.

III. Flight Tests of the JPL VCM Waveform using the SCaN Testbed

A. Test Goals

The main objective of the flight test was to demonstrate technology capability and readiness of the JPL VCM waveform using an S-band link between the SCaN testbed and the ground antenna at GRC. The dynamic feature of the ISS link due to various interference effects (e.g., multipath loss, obstructions, and pointing), provides a real-world environment in which to validate and evaluate the capability and effectiveness of VCM methods. The test can be declared a success if decodable data are obtained throughout most of the scheduled VCM mode transitions. A second goal, if the link condition permits, is to demonstrate that significant improvement in data throughput can be achieved using the VCM waveform as compared to a traditional NASA waveform. In addition, we want to verify the capabilities of JPL's VCM receiver tools that were developed to autonomously acquire, track, and recover information data transmitted using the VCM protocol. The flight test serves as a milestone in achieving a higher level of the technology readiness for the JPL VCM waveform.

B. Test Facilities and Equipment

The SCaN Testbed [12] is an advanced integrated communications system and laboratory facility installed onboard the ISS. It provides researchers a platform to develop,

test, and demonstrate new communications, networking, and navigation capabilities in the actual environment of space. Payload operations are executed from the Control Center at Glenn Research Center (GRC) in Cleveland, Ohio. The operating systems and waveforms on the SDRs are reconfigurable and are used to perform experiments by uploading and executing new waveforms. In this test we utilized the JPL SDR on the SCaN Testbed and the direct-to-Earth S-band communication link between the ISS and the GRC ground station to validate and evaluate JPL’s VCM waveform technology.

1. JPL SDR on the SCaN Testbed

Figure 3 shows the block diagram of the JPL SDR platform on the SCaN Testbed [6,13]. It consists of two main modules: a signal processing module and an RF module.

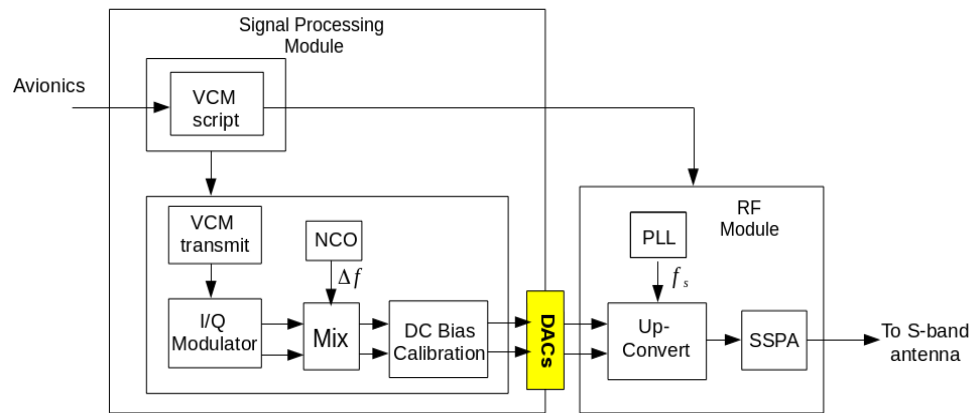


Figure 3. Block Diagram of the JPL SDR.

The software unit of the signal processing module configures VCM modes, the carrier frequency in the phase-locked loops (PLL), and the solid-state power amplifier (SSPA) transmit power. The signal processing module interfaces with the flight computer (avionics) and handles the VCM scripts to configure and control the radio. In our test of the current JPL VCM waveform, the software also performs encoding and bit randomization. The FPGA firmware frames and modulates the encoded data stream, mixes with the frequency offset Δf , adjusts for DC offset, and performs digital-to-analog conversion. The RF module up-converts the signal to the SDR’s RF at f_s , amplifies it by the SSPA with power level configured by VCM software, and eventually radiates it out of the S-band antenna.

2. GRC Ground Station and Experimental Arrangement

The S-band ground station is located at GRC. A block diagram of our experimental arrangement at GRC is shown in Figure 4.

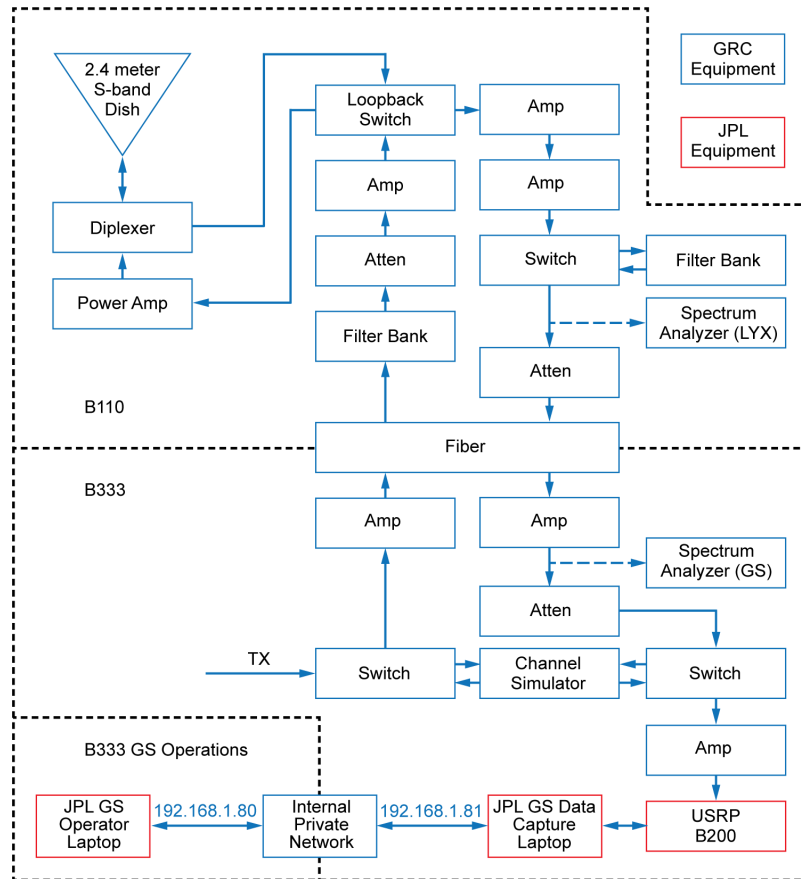


Figure 4. Experimental arrangement at GRC.

It contains a steerable antenna, various power meters, spectrum analyzers, and an RF-over-fiber system between buildings B110 and B333. Automatic gain control (AGC) was also used to set an attenuator between the GRC Ground Station (GRC-GS) and JPL’s experimental equipment to avoid saturation. The GRC-GS is the ground element of the SCaN Testbed that performs payload operations to support test and validation of new technology development. Before the scheduled flight test, we utilized GRC’s engineering model (EM) of the SCaN Testbed, i.e., the ground integration unit (GIU), to perform final verification tests of the JPL VCM waveform.

In Figure 4, the blocks in orange are JPL equipment components connected to the front-end of the GRC ground receiver. JPL’s test equipment consists of a universal software radio peripheral (USRP), a high-performance Linux laptop with GNU Radio¹ software installed, and a laptop to remotely control the GNU Radio laptop. The USRP takes the RF signal received by the GRC ground receiver, down-converts it to baseband, performs analog-to-digital conversion, and outputs raw I/Q samples to the GNU Radio laptop.

¹GNU Radio is a free and open-source development tool that provides signal-processing blocks to implement software radios.

We set the USRP center frequency at 2216.5 MHz (the S-band center frequency f_c), and sampling rate at 3.0778 MHz. The GNU Radio receiver tool on the Linux laptop was used both as an open-loop recording tool to save raw I/Q samples for post-processing, and as a real time receiving tool to quickly check whether the ground station had been configured properly to receive the RF downlink data. In addition to JPL’s GNU Radio receiver tool, we also used GRC’s Spectrum Analyzer for real time monitoring of the spectrum and to estimate the signal-to-noise ratio (SNR) of the received signal. The power reading and time log from GRC’s Spectrum Analyzer provided information for us to estimate the actual received SNR during the communication session.

C. JPL Ground Station Receiver Tools

The USRP takes the RF signal fed from the front-end of GRC’s ground receiver, down-converts it to complex baseband, and samples at 3.0778 MHz with 32-bit quantization. The raw I/Q samples are interleaved and saved in a file for post-processing and performance analysis. We developed GNU Radio receiver tools for tracking and demodulation of the raw sample data. An example of this tracking/demodulation processing chain is shown in Figure 5.

The main blocks of the receiver chain include an AGC, a Costas loop for carrier tracking, and a symbol tracking loop to recover symbol timing. The configuration parameters of the receiver are tuned during post-processing to ensure data recovery. There are also various auxiliary blocks such as the frequency sink, the constellation sink, and the ASM header detection, which allow us to visually inspect acquired symbols and VCM PL frame payload content. These utilities provided capabilities for real-time monitoring of anomalies in the received data. The quick-check capability of the tool allows us to select and tune the parameters of receiver blocks to ensure that the tracking loops are in lock.

The acquired modulation symbols are then sent to a VCM frame processing tool which processes the VCM frames and performs validation of payload data content. The VCM frame processing tool performs frame synchronization, VCM frame descriptor decoding/extraction, mapping of the I/Q values to soft symbols, de-randomization, and decoding.

For BPSK and QPSK, the mapping function that transforms the acquired I/Q values into soft symbols is straightforward. For 8-PSK, we adopted a slight variation of the maximum likelihood mapping function used in [14] for a constellation with Gray code mapping. The modulation symbols are first rotated clockwise by $\pi/8$ radians and then mapped to soft symbols as follows: Let $\{\lambda_2, \lambda_1, \lambda_0\}$ be the soft symbols, and $\{I, Q\}$ be the modulation symbol pairs, we have

$$\begin{aligned}\lambda_2 &= \frac{1}{\sqrt{2}}(|I| - |Q|) \\ \lambda_1 &= \frac{1}{\sqrt{2}}I \\ \lambda_0 &= \frac{1}{\sqrt{2}}Q.\end{aligned}$$

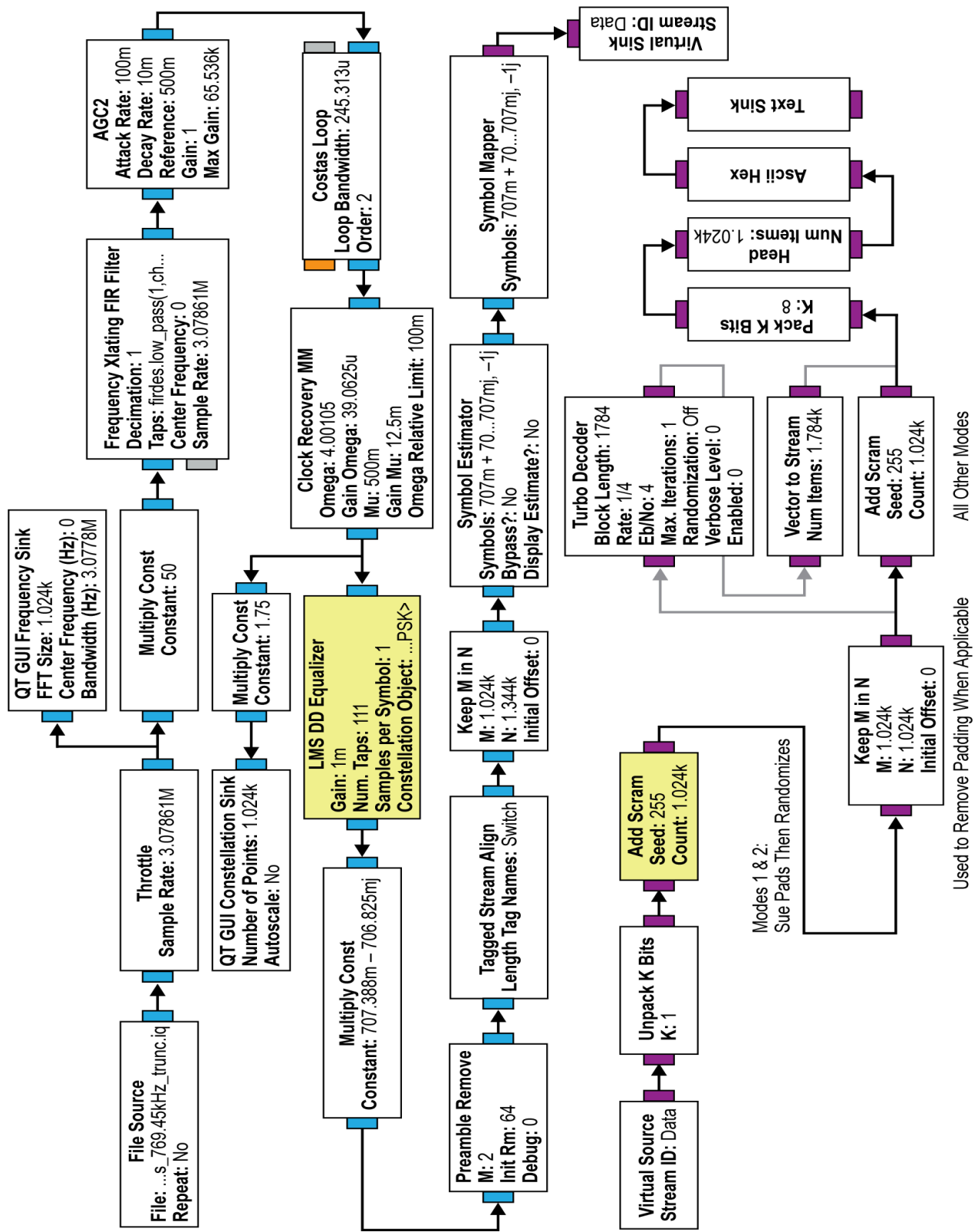


Figure 5. GNU Radio Receiver Configuration used for open-loop recording and post-processing.

The soft symbols are then de-randomized and fed to the decoder for soft decoding. The output of the VCM frame processing tool is a stream of information bits which are then compared with the test pattern to obtain performance metrics such as frame error rates or bit error rates.

IV. Flight Test Results

A. Link Prediction

A few days prior to the scheduled flight test, GRC’s SCaN Testbed Analysis Tool (STAT) was used to produce the latest SNR predicts for all of the scheduled events. We used the SNR predicts to select passes and to design VCM mode sequences for each of the selected passes. On the day of the selected pass, an updated predict was produced by GRC to account for the latest ISS events that could cause changes in the link. We adjusted the JPL SDR VCM script with timed VCM mode transitions to accommodate the latest SNR predicts. This script was uploaded to the ISS avionics to configure the SDR and trigger data transmission at the commanded time.

A sample STAT link budget for an ISS pass is presented in Table 2. For all the predicts we used in the flight test, a constant pointing loss (i.e., 2 dB) was assumed. However, as noted in [6], the open-loop pointing error of the receiver antenna increases as a function of the elevation angle. This would lead to deviations of the predicted SNR from the actual received SNR, especially at high elevation angles. In our VCM mode sequence design, we left the link margin as is to accommodate this pointing uncertainty.

Table 2. Sample link budget for an ISS-GRC pass.

Parameter	Value	Notes
Transmit Frequency	2216.5 (MHz)	
(1) Transmit Power	7.5 (dBW)	
(2) Transmit Antenna Gain	3.05 (dBi)	at 10° elevation angle
(3) RF Subsystem Loss	-1.7 dB	
(4) EIRP	8.86 (dBW)	(1) + (2) + (3)
(5) Free Space Loss	-164.26 (dB)	
(6) Atmospheric Loss	0	
(7) GS Pointing Loss	-2 (dB)	assumed in STAT model
(8) G/T	-8.41 (dB/K)	at 10° elevation angle
(9) Boltzman’s Constant	228.6 dBW/K/Hz	
(10) P_d/N_0 at Receiver	62.8 (dB-Hz)	(4) + (5) + (6) + (7) + (8) + (9)

B. Ground Integration Unit Test

The day before the flight test, several ground integration tests were conducted utilizing the GIU simulator at GRC. The goal of the ground integration tests was to verify that the JPL ground station equipment was properly connected to the GRC ground station, and that JPL’s GNU Radio receiver captured the RF data at the expected power levels. The JPL equipment was then connected to the GRC ground receiver as in Figure 4 in preparation for the first flight test. The JPL SDR was powered on and the VCM waveform files (FPGA bitfile and GPP SPARC image) were uploaded to the SCA_N Testbed avionics.

C. DAY 1 - Pass event A2

The passes on day 1 did not include the 17-leap-seconds adjustment that should have been added to the avionics script start time to align it with the Coordinated Universal Time (UTC) pass start time. This adjustment is needed because the avionics time uses the straight Global Positioning System (GPS) time without the GPS leap seconds applied. This resulted in a misalignment between the link SNR profile and the VCM SNR profile. Since the VCM SNR profile typically rises and then sets to align with the signature of the link profile, this time misalignment can lead to operating the link with negative margin at the beginning of the pass.

Table 3 shows the timeline information of tracking pass A2 on day 1, including the predicted obstruction start time. The total unobstructed duration of this pass is about 225 seconds.

Table 3. Timeline information for pass event A2.

Event	Date	Start Time	End Time	Overall Duration	Unobstructed End
A2	6/19/2017	16:19:15	16:27:01	0:07:46	16:23:00

Figure 6 shows the predicted, received, and required SNRs for this pass. The predicts were produced by GRC’s STAT link analysis tool in the morning of the scheduled event. We designed the VCM mode profile based on the latest predicts. The red staircase line in Figure 6 shows the required SNR and the transmission duration for each mode. The actual SNR was calculated from the received power log that was recorded by GRC’s Spectrum Analyzer. In this plot, we shifted our scheduled VCM SNR profile (red line) by 17 seconds to account for the aforementioned timing misalignment.

Besides the timing misalignment issue, the script on day 1 did not incorporate the correct I/Q calibration values for the SDR flight model. As we explained in Section II, this miscalibration caused CW interference in the received signal and led to performance degradations. Figure 7 shows the spectrum of the received signal after down-conversion. The CW interference tone at frequency offset $\Delta f = 285$ kHz is clearly present in the received signal.

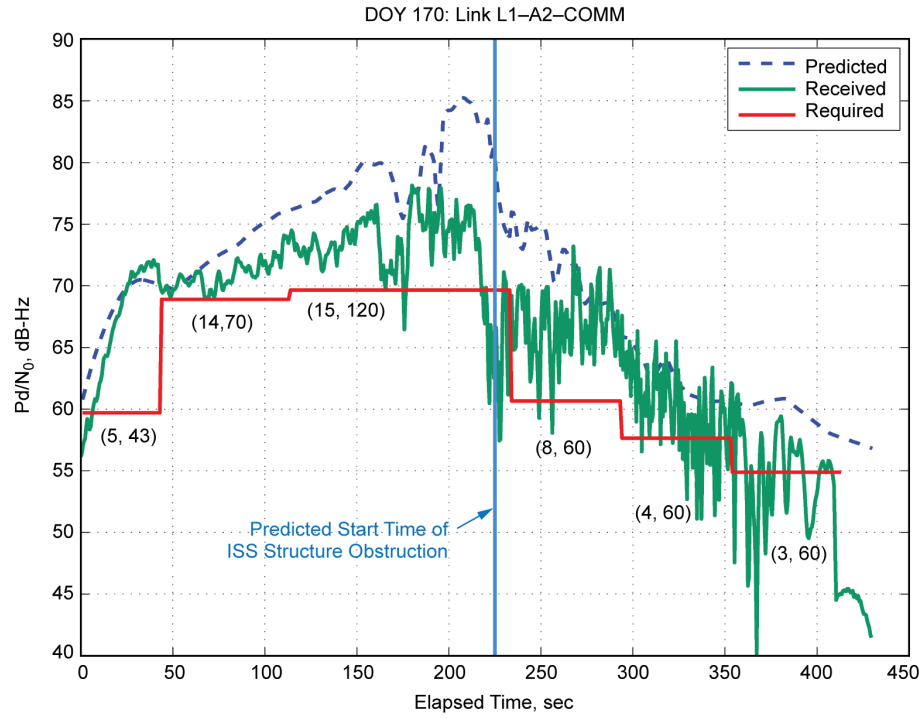


Figure 6. Predicted, received, and required SNR profile for pass A2 on Day 1. The number pairs below the red curve represent the VCM modes and associated transmission durations over six pass sections.

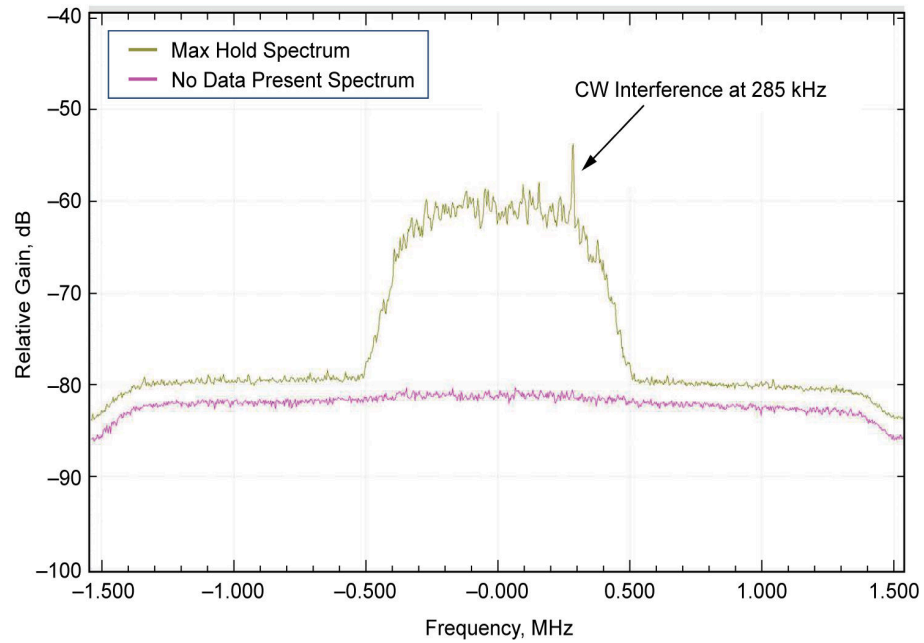


Figure 7. Spectrum of the received signal. The light green curve was produced by Max Hold mode of the spectrum analyzer, capturing the data spectrum. The magenta curve is the spectrum of a segment where no data were present. CW interference tone at $\Delta f = 285$ kHz is due to uncalibrated DC offset.

The effects of CW interference on the tracking loop vary as the link conditions change. When the noise level exceeds a certain threshold (e.g., during the beginning and end of the pass), the desired signal cannot be tracked. Conversely, when link SNR increases, the tracking loop is able to reach a steady state and acquire the signal. As an example, in Figures 8 and 9 we plotted the symbol constellations that were obtained under both scenarios for mode 5 in this pass.

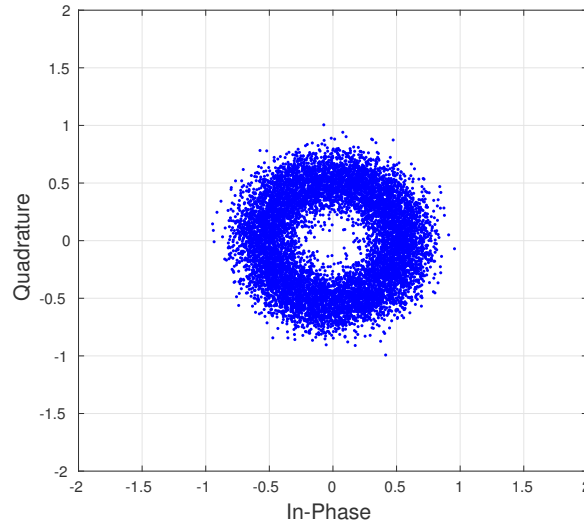


Figure 8. Constellation plots of reconstructed symbols from mode 5 of event A2. Tracking loop is out of lock.

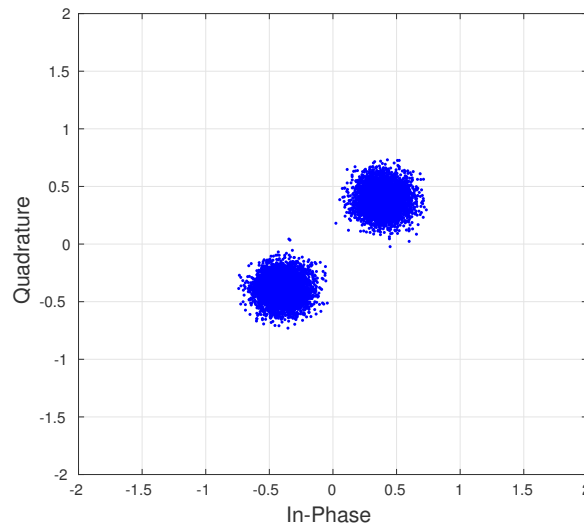


Figure 9. Constellation plots of reconstructed symbols from mode 5 of event A2. Tracking loop is in lock.

Table 4 summarizes the data loss analysis results of this pass. We reported the number of VCM PL frames that we were able to acquire, the duration of the acquired frames, the originally planned duration for each mode, and the code word error rate (CWER) for the

acquired frames. There were significant data losses in this pass due to CW interference before the obstruction started. The performance deteriorated further afterwards due to the combined effects of low SNR and CW interference.

Table 4. Summary of data loss analysis for pass A2.

Section of pass	Mode	Acquired no. of frames	In-lock duration (sec)	Planned duration (sec)	CWER of acquired frames
1	5	11882	28.67	43	2.5e-4
2	14	69440	67.42	70	0.2706
3	15	28251	111.62	120	0.177
4	8	4307	7.52	60	0.0306
5	4	13214	40.67	60	0.4659
6	3	858	6.35	60	0.5711

To prevent this problem from occurring in future tests, we obtained the I/Q calibration values from the GRC team who had performed calibration in their JPL-GGT 2.0 VCM test [6] using the Flight Module (FM). These calibrations values were used in our software for the subsequent events

D. DAY 2 - Pass event A11

There were a total of four scheduled passes for Day 2. However only one of the passes, which we named A11, was properly recorded. In this section we focus on the performance analysis results of pass A11. Table 5 shows the turbo information of event A11, including predicted obstruction start time. The total unobstructed duration of this pass was about 228 seconds.

Table 5. Timeline information for pass event A11.

Event	Date	Start Time	End Time	Overall Duration	Unobstructed End
A11	6/20/2017	21:55:17	22:03:04	0:07:47	21:59:05

Figure 10 shows the predicted, received, and required SNRs for this pass. We adjusted the VCM profile (red line in Figure 10) based on the latest predicts obtained in the morning. The updated VCM script, with the correct I/Q calibration parameters, was uploaded to the SCA_N testbed before the scheduled event time. The gap between the actual SNR (green curve) and the required SNR (red curve) of the sequenced VCM modes indicates the link margin for this pass.

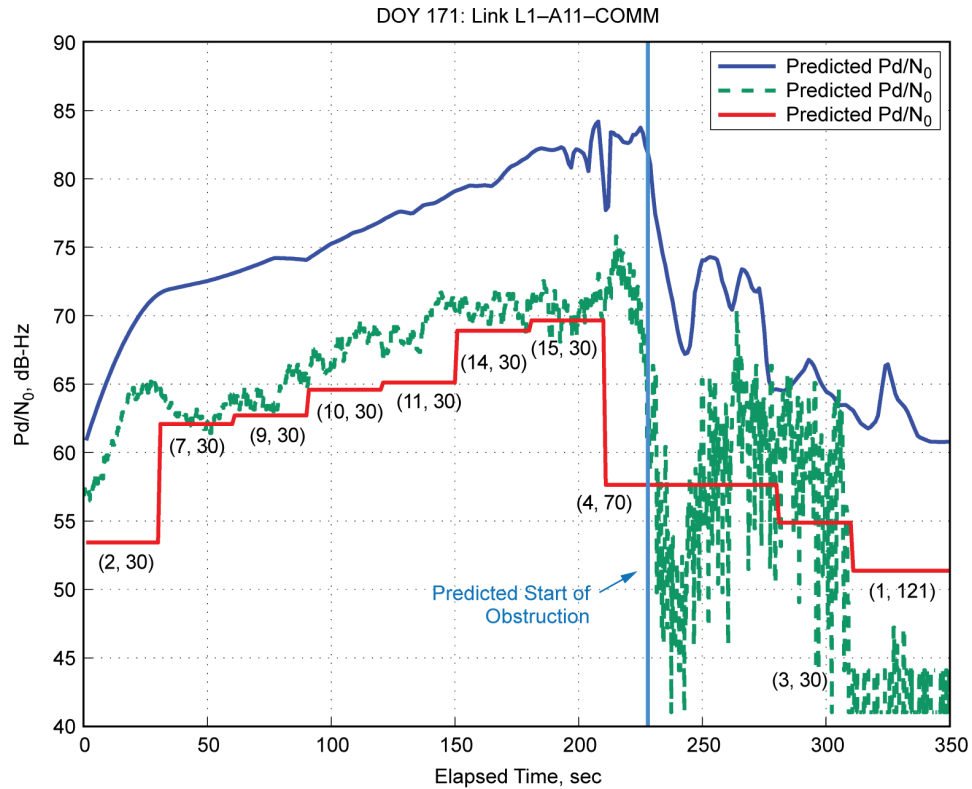


Figure 10. Predicted, received, and required SNRs for pass A11. The pairs of numbers below the red curve represent the VCM modes and associated transmission duration for each section of the pass.

The SNR took a dive after obstruction began occurring at about 228 seconds into the pass. The VCM modes scheduled for transmission after the obstruction experienced significantly higher frame losses. In the performance analysis we focused on the first eight modes of the VCM sequence that were scheduled and transmitted during the unobstructed period of the pass.

The recorded complex baseband samples were post-processed by the GNU Radio receiver tool for carrier and symbol acquisition. Initial phase ambiguity resolution was performed by aligning the VCM symbol constellation with the known BPSK constellation of the ASM bits. The receiver configuration, including loop filter bandwidth and AGC parameters, was tuned during post-processing to ensure that the tracking loops remained in lock. Additional adjustment and optimization of these parameters can potentially improve the receiver performance. However, the details are beyond the scope of this report.

Figure 11 shows examples of constellation plots of the acquired symbols from the eight VCM modes tested during this pass before the start of obstruction.

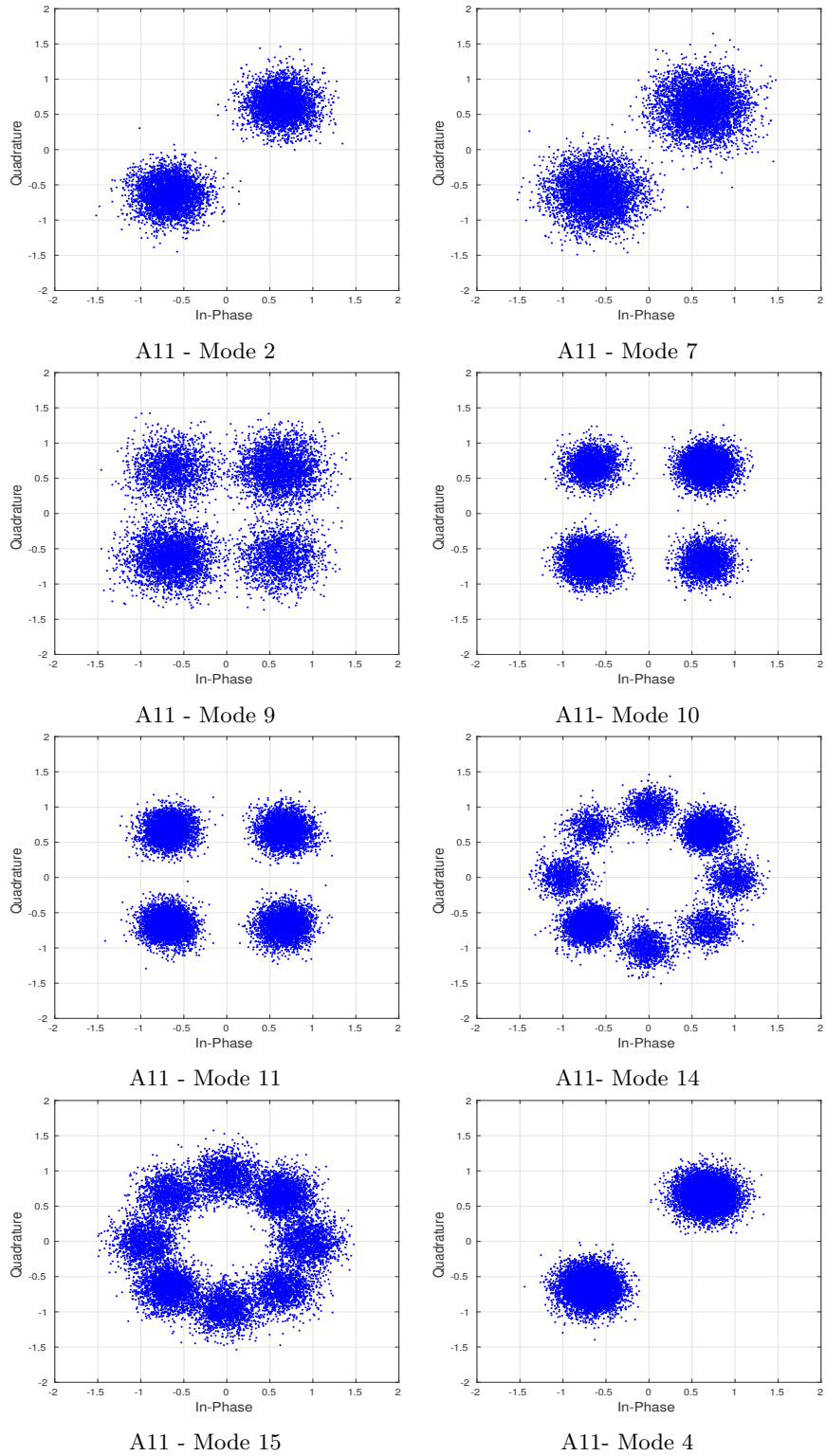


Figure 11. Constellation plots of acquired symbols from modes 2, 7, 9, 10, 11, 14, 15, and 4 of event A11.

The output of the GNU Radio receiver consists of streams of interleaved I/Q symbols. These symbols are passed to the VCM frame processing tool that performs frame synchronization, VCM mode detection, mapping to soft symbols, derandomization, and decoding. The VCM frame processing culminated in a sequence of information bits, which are compared with the test patterns to obtain error rate statistics. Figure 12 shows the ASM frame cross-correlation plot in the beginning of the pass. Only VCM modes 2 and 0 were active during this period.

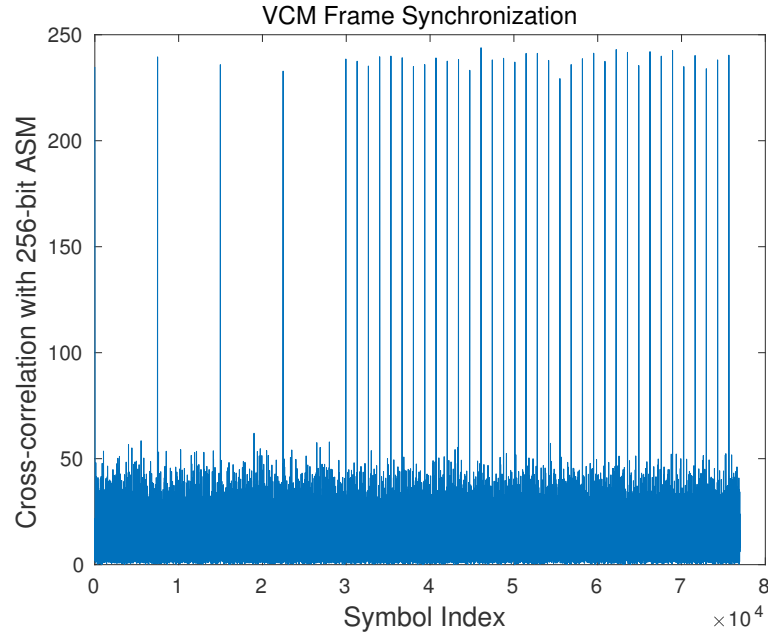


Figure 12. Cross-correlation with the 256-bit ASM during a VCM mode transition (mode 2 to mode 0) of pass A11.

Table 6 summarizes the performance analysis results from the received data for this pass. In this table we report for each mode, the relative percentage of transmission, average information data rate (kbps), required and actual symbol SNR, and codeword error rate (CWER).

VCM frames transmitted during the first six pass sections (modes 2, 7, 9, 10, 11, 14) were reconstructed error-free. There was a single codeword error that occurred among all reconstructed mode 15 frames (pass section 7 as shown in Figure 13). The green curve represents average bit error rates before decoding, obtained by simply hard thresholding the received VCM soft symbols. This indicates the noise level of the channel as a function of time. The red dot indicates a single frame error where the decoder failed to decode the codeword. Figure 14 is a plot of the bit error rate, calculated per information block, for decoded mode 4 frames (pass section 8). The mode 4 frames were successfully reconstructed until the obstruction started. At this point, the link SNR dropped significantly below the value required by the decoder, causing a significant increase in codeword error rates.

Table 6. Summary of performance analysis of pass A11.

Section of pass	Mode	Bits per Channel use	Data Rate (kbps)	Required E_s/N_0 (dB)	Received E_s/N_0^* (dB)	CWER	Percent Time
1	2	0.25	192.36	-5.42	0.98	0	8.24
2	7	0.8745	672.88	3.24	4.76	0	13.17
3	9	1	769.45	1.8	4.76	0	12.46
4	10	1.6	1231.12	5.73	7.58	0	12.99
5	11	1.75	1346.54	6.25	9.46	0	11.73
6	14	2.4	1846.68	10.05	11.81	0	12.47
7	15	2.62	2015.96	10.79	11.67	1.69e-4	10.75
8	4	0.5	384.83	-1.21	13.04	0.1490	8.89
**	0	1	769.45	8.4		N/A	9.30

* The average received symbol SNR is shown for each mode duration. There are significant variations in the received power during the pass.

** There are multiple sections of mode 0 frames inserted between the other VCM modes. We counted all mode 0 frames together as an overhead in the transmission.

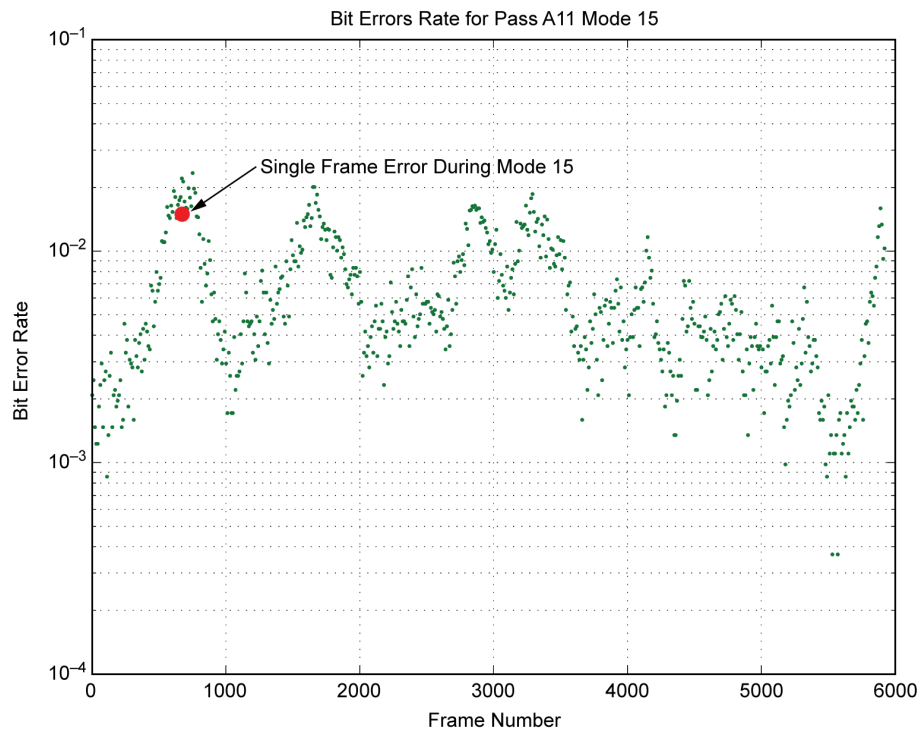


Figure 13. Bit Error Rates in received VCM mode 15 frames during pass A11.

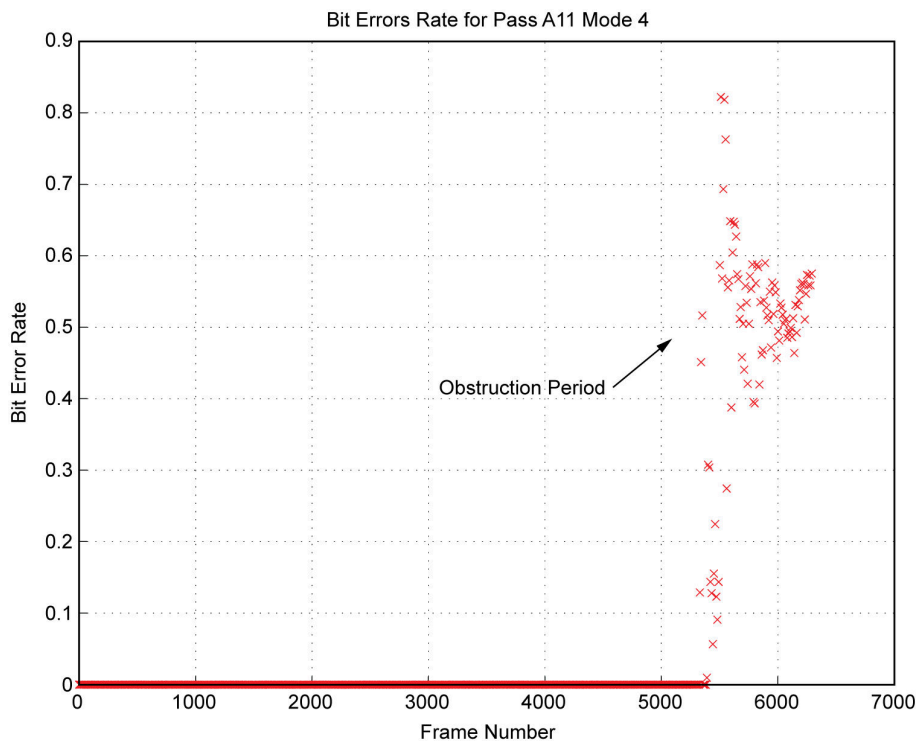


Figure 14. Bit Error Rate in reconstructed VCM mode 4 frames during pass A11.

We considered mode 0 frames as overhead in our analysis because insertion of mode 0 frames was simply due to software limitations in our current waveform design. We verified that all VCM modes switched successfully as commanded from the VCM script. Furthermore we verified that no frame loss occurred during mode transitions. The overall information data volume received error free for this pass is 217.17 Mbits. The standard NASA waveform, which uses QPSK modulation with concatenated inner (7,1/2) convolutional code and outer (255,223) Reed-Solomon code, would require a symbol SNR E_s/N_0 of 2.59 dB to achieve a bit error rate of 10^{-6} . The link duration satisfying this requirement is about 204 seconds, which leads to a total data volume return of 137.27 Mbits if the standard NASA waveform was used. The overall improvement achieved by the VCM method in data volume return for this pass is about 1.99 dB. Note that our VCM waveform incurred about a 0.32dB penalty due to the overhead of mode 0 frame insertion in the transmitted streams. We plan to resolve this in our next VCM waveform version.

V. Future Work Recommendations

This project was cancelled a year early due to budgetary issues in the ScaN Technology Program. The flight test clearly demonstrated the efficacy of the JPL VCM waveform and the promise of significant future link performance improvements, yet we did not have the opportunity to flight test the FPGA coding that was developed and lab tested

after the ISS flight test. We also did not have the opportunity to continue into the next phase in which we were planning to add disruption tolerant networking (DTN) to the JPL SDR, and to demonstrate the automatic control of the VCM mode using the DTN Licklider Transmission Protocol (LTP) [15] to infer link SNR status.

Completing the SDR work and proving out the VCM concept, as well as adding the automatic control of VCM modes, would provide a solid technology that would be directly transferrable to other future radio hardware implementations such as the universal space transponder (UST) or the Iris radio.

The current NASA directive to infuse DTN into all three NASA communications networks in the next few years makes a continuation of this research and, if possible, another ISS flight test sometime in 2018, very synergistic propositions. The authors recommend the addition of a VCM/ACM/DTN-enabled radio system to the end-to-end DTN space internetworking foundation of cognitive networking.

VI. Conclusions

A series of tests on JPL's VCM waveform were conducted using the SCaN Testbed on board the ISS. The JPL SDR was able to successfully switch to different VCM modes as configured to match predicted link conditions. We developed VCM ground receiver tools to post-process and reconstruct information data from the received VCM frames. Performance analysis results show significant improvement achieved by VCM methods as compared to the NASA standard waveform.

Acknowledgments

The authors are pleased to acknowledge Michael Evans, Maria Piasecki, Beth Curtis, and Al Rybar of Glenn Research Center, for helping and conducting the tests at GRC.

References

- [1] *TM Synchronization and Channel Coding*, Consultative Committee for Space Data Systems (CCSDS) 131.0-B-2, Blue Book, August 2011.
- [2] *Radio Frequency and Modulation Systems—Part 1: Earth System Standards*, Consultative Committee for Space Data Systems (CCSDS) 401.0-B-23, Blue Book, September 2003.
- [3] *Flexible Advanced Coding and Modulation Scheme for High Rate Telemetry Applications*, Consultative Committee for Space Data Systems (CCSDS) 131.2-B-1, Blue Book, March 2012.
- [4] *Space Link Protocols over ETSI DVB-S2 Standard*, Consultative Committee for Space Data Systems (CCSDS) 131.3-B-1, Blue Book, March 2013.
- [5] *Digital Video Broadcasting (DVB): Second Generation Framing Structure, Channel Coding and Modulation Systems for Broadcasting, Interactive Services, News Gathering and*

other Broadband Satellite Applications, ETSI EN 302 307, V 1.2.1. European Broadcasting Union, 2009.

- [6] J. A. Downey, D. J. Mortensen, M. A. Evans, and N. S. Tollis, “Variable Coding and Modulation Experiment Using NASA’s Space Communication and Navigation Testbed,” *International Communications Satellite Systems Conference*, October 2016.
- [7] *Variable Coded Modulation Protocol*, Consultative Committee for Space Data Systems (CCSDS) 131.1-R-0.1.3, Red Book, April 2015.
- [8] W. Fong, S. Lin, G. Maki, and P. S. Yeh, “Low Density Parity Check Codes: Bandwidth Efficient Channel Coding,” in *NASA Earth Science Technology Conference*, 2003.
- [9] *Telemetry Channel Coding*, Consultative Committee for Space Data Systems (CCSDS) 101.0-B-4, Blue Book, May 1999.
- [10] C. Y. Yoon and W. C. Lindsey, “Phase-locked Loop Performance in the Presence of CW Interference and Additive Noise,” *IEEE Transactions on Communications*, vol. 30, no. 10, pp. 2305–2311, October 1982.
- [11] M. F. Karsi and W. C. Lindsey, “Effects of CW Interference on Phase-locked Loop Performance,” *IEEE Transactions on Communications*, vol. 48, no. 5, pp. 886–896, May 2000.
- [12] “SCaN Testbed Systems,” Glenn Research Center, Cleveland, Ohio, <https://spaceflight systems.grc.nasa.gov/sopo/scsmo/scan-testbed/>.
- [13] R. C. Reinhart and J. P. Lux, “Space-based Reconfigurable Software Defined Radio Testbed aboard International Space Station,” in *AIAA Space Ops Conference*, Pasadena, California, United States, May 2014.
- [14] M. Cheng, D. Divsalar, and S. Duy, “Structured Low-Density-Parity-Check Codes with Bandwidth Efficient Modulation,” *Proceedings of SPIE*, vol. 7349, May 2009.
- [15] *LICKLIDER Transmission Protocol (LTP) for CCSDS*, Consultative Committee for Space Data Systems (CCSDS) 734.1-B-1, Blue Book, May 2015.